Energy harvesting analysis of hip implantin achieving sustainable development goals

Oladapo, Bankole I.; Bowoto, Oluwole K.; Adebiyi, Victor A.; Ikumapayi, Omolayo M.

DOI:
10.1016/j.istruc.2023.05.150

Publication date:
2023

Structures 55 (2023) 28–38

Contents lists available at ScienceDirect

Structures

journal homepage: www.elsevier.com/locate/structures

Energy harvesting analysis of hip implantin achieving sustainable development goals

Bankole I. Oladapo [a,b,*], Oluwole K. Bowoto [c], Victor A. Adebiyi [d], Omolayo M. Ikumapayi [e]

[a] School of Science and Engineering, University of Dundee, Dundee, United Kingdom
[b] Sustainable Development, De Montfort University, Leicester, United Kingdom
[c] University of Bolton, Department of Mechanical Engineering, Bolton, United Kingdom
[d] Centre for Agroecology, Water and Resilience (CAWR), Coventry University, Department: Fundamental Processes and Resilience, United Kingdom
[e] Mechanical Mechatronics Engineering, Afe Babalola University, Ado-Ekiti, Nigeria

ARTICLE INFO

Keywords:
Energy-harvesting
Piezoelectric
Hip prosthesis
Finite element analysis
Sustainable healthcare solutions
Autonomous implants

ABSTRACT

In line with the United Nations' Sustainable Development Goal 3, promoting good health and well-being, this study explores a novel approach to energy-harvesting autonomous implants for intelligent orthopaedic solutions. Addressing the challenge of providing a reliable and easily accessible power source for active mechanical components and investigating piezoelectric hip prostheses' design and performance. The modified hip implant incorporates three vibration-based harvesters running in parallel, capturing energy during an average human stride through angular movements such as flexion, extension, and abduction. Finite element analysis is utilised to evaluate structural stress failure strength and refine the implant design, ensuring enhanced load transfer to the piezoelectric element and increased energy generation. The experimental results demonstrate the potential to harvest up to 55 J/s of helpful power and 1.76 V, contributing to the development of sustainable and reliable intelligent hip implants that can operate continuously without being disabled and work without risk. This innovative approach supports advancements in healthcare technology and improved patient outcomes, emphasising the importance of sustainable and accessible solutions in the orthopaedic field. Future research will delve into energy conversion and fatigue in complete hip implant designs, further promoting health, well-being, and sustainability in healthcare solutions.

1. Introduction

Surgical revision remains the primary treatment for most total joint replacement failures. While antimicrobial medication, suppressive antibiotic therapy, outpatient parenteral antimicrobial therapy, and antibiotic prophylaxis can delay common replacement failure, they cannot prevent it [1–3]. These surgical revisions alleviate pain and enhance joint function but fail to address or prevent early shortcomings. Improving prosthesis functionality often necessitates exploring innovative designs, materials, attachment methods, and surgical procedures [4–6], aligning with the United Nations Sustainable Development Goal (SDG) 3: Good Health and Well-being. With an increasing global population and technological advances, there is a growing demand for primary and revision joint replacements. The revision rate for orthopaedic prostheses after 20 years remains over 20% [7,8], emphasising the need for durable prostheses for people under 65 who are hospitalised for joint disorders [9,10]. This highlights the importance of investing in research and development to support SDG 9: Industry, Innovation, and Infrastructure. Current hip prostheses are passive, and while instrumented prostheses introduced in the 1960s have helped improve passive implants, surgical operations, preclinical testing, and physiotherapy programs, they still lack a reliable method to generate power [11–23]. Developing innovative hip implant circuitry that efficiently manages power and harnesses energy from a person's movements to power intelligent hip prostheses could contribute to SDG 7: Affordable and Clean Energy.

As the world's population continues to grow and younger individuals receive implants, the incidence of failing implants will increase proportionally to original arthroplasties [24–26]. This emphasises the need for novel treatments and technologies in the future, which could help address deficiencies and expand the range of available treatments. Diagnostic sensors can track implant stability, loosening, or wear to

* Corresponding author at: School of Science and Engineering, University of Dundee, Dundee, United Kingdom.
E-mail address: boladapo001@dundee.ac.uk (B.I. Oladapo).

https://doi.org/10.1016/j.istruc.2023.05.150
Received 31 January 2023; Received in revised form 28 May 2023; Accepted 30 May 2023
Available online 12 June 2023

inform corrective actions. In contrast, active sensors can promote bone formation and implant life [27–29]. Such advancements align with SDG 3: Good Health and Well-being by reducing the need for invasive, costly, and potentially life-altering revision surgeries, and SDG 9: Industry, Innovation, and Infrastructure by promoting technological progress in orthopaedic implants. Active sensors, such as electrical stimulation, have the potential to stimulate bone formation and extend implant life. Optimal power supplies are crucial for these sensors and actuators. Data and electricity have been transmitted through the infected percutaneously, allowing for wireless measurements through telemetry and batteries [30–32]. However, batteries have limitations, such as a short lifespan and leakage issues. Inductive coupling can address these challenges but is limited to clinical or laboratory settings due to the need for external equipment. Energy harvesting offers a promising solution, aligning with the United Nations Sustainable Development Goal (SDG) 7: Affordable and Clean Energy [33,34]. Using energy harvesting, instrumented implants can generate their power source, eliminating the need for replacements and ensuring continuous operation. Implant loads can be transmitted to a multilayer piezoelectric element through the hip implant and UHMW-PE housing [35–37], creating a self-powered sensor that generates electricity during physical activity. This research aims to develop and test a prototype device that uses vibration analysis to assess implant stability, which is expected to be more user-friendly, compact, and cost-effective for clinical applications. This aligns with SDG 9: Industry, Innovation, and Infrastructure.

Additionally, this study proposes installing piezoelectric devices in mechanically loaded areas to produce electricity, which requires careful placement to minimise the impact on the hip implant's cross-sectional area and forces, thereby preserving the implant's longevity. By examining the safety of a mechanically stressed metal hip implant component, this research contributes to SDG 3: Good Health and Well-being. Using finite element analysis (FEA) and load testing, this study also aims to determine a PLA hip implant's worst-case structural fatigue failure strength, which will provide valuable insights into implant design improvement. By surpassing the ISO requirement and conducting further FEA to understand stress distribution, this research supports SDG 9: Industry, Innovation, and Infrastructure by promoting technological progress in orthopaedic implants. Ultimately, these advancements will contribute to better patient outcomes, reduced healthcare costs, and improved overall well-being, aligning with SDG 3: Good Health and Well-being.

2. Methodology

In this study, we aimed to develop a new hip implant using sustainable materials and innovative design principles, aligning with the United Nations Sustainable Development Goal (SDG) 9: Industry, Innovation, and Infrastructure. We 3D printed the hip implant with filament purchased from ZHUHAI JIAWEI IMPORT AND EXPORT TRADING CO LTD. We selected the V40 PLA offset head with an 8-mm offset and mounted a linear strain gauge to the hip implant chamber's side for Finite Element Analysis (FEA) validation. We utilised a template to adjust the sensor's centre and measurement direction axis, ensuring a consistent strain gauge installation that worked with the FE model. The simulation results met the requirements for an evenly loaded region and a location near the target zone. However, the curved shape of the hollow base's projected stress concentration proved unsuitable for strain gauges. We followed the ISO standard 7206–4 for testing and aligned three hip implant specimens using an aligning fixture of 9° to 10°. We positioned the sample before electrodynamic uniaxial testing equipment with a 5 kN load cell and soft springs that maintained a ball ring between the head and the piezoelectric materials to prevent side forces. During a quasi-static experiment, we gradually increased the load to 2300 N in 10 stages and monitored stresses using a strain gauge. We applied each load level thrice for 5 s and calculated the average strain for each location. We tested three samples with a maximum sinusoidal load of 2300 N, R = 0.1, 10 Hz, and million cycles. After five million cycles, we increased the load by 300 N per million cycles (R = 0.1) until failure. We removed the sample from the machine after 5 million cycles to allow the ball ring to return. Fig. 1 illustrates the testing strategy of boundary conditions Ux and loading of the FEA model femoral head centre with fixed support in red. Strain gauge local coordinate grid detail. By investigating this new hip implant's structural properties and fatigue failure strength, we contribute to SDG 3: Good Health and Well-being by promoting advancements in orthopaedic implants that improve patient outcomes, reduce healthcare costs, and enhance overall well-being. Our innovative approach to hip implant development and testing supports SDG 9: Industry, Innovation, and Infrastructure by fostering progress in orthopaedic implant technologies.

In this study, we aimed to develop a patient-specific PLA 3D-printed hip implant by using a commercially available hip implant as a starting point. The revised design allowed for the integration of electronics without compromising the structural integrity of the device. This innovation aligns with the United Nations Sustainable Development Goal (SDG) 9: Industry, Innovation, and Infrastructure. We relocated the control unit to a cassette incorporated into the overall design, using a 3 V lithium coin battery to power the ultra-low-power 2.4 GHz RF transceiver. We monitored the implant using an external accelerometer comprising an additional RF chip and a microcontroller. The microcontroller received data from sensors connected to a Serial Peripheral Interface via Bluetooth. To test the communication technology in a realistic environment, we wirelessly collected data from a distance of 2 m. Fig. 2 depicts the 3D-printed model and enclosure for the monitoring equipment. It is important to note that the proposed system has not been tested in-vivo or in-vitro to demonstrate its ability to detect loosening. We conducted the experiment using three separate samples. By exploring the feasibility of a patient-specific PLA 3D-printed hip implant with integrated electronics, we contribute to SDG 3: Good Health and Well-being by promoting advancements in orthopaedic implants that improve patient outcomes, reduce healthcare costs, and enhance overall well-being. Furthermore, our innovative approach to hip implant development and testing supports SDG 9: Industry, Innovation, and Infrastructure by fostering progress in orthopaedic implant technologies.

3. Finite element analysis

The hip implant's finite element analysis (FEA) was performed to replicate the quasi-static testing accurately. We used Autodesk Inventor 2023 to create the geometry and imported it into ANSYS 2022 (Ansys Inc, USA). The only modifications made were to the hip implant and embedding. A strain gauge measurement grid and a local coordinate system were established on the lateral implant region, with the x-axis oriented in the measurement direction. The force was applied to the centre point of the head, which then propagated to the outer surface of the taper. The cylindrical axis of the embedding material was loaded, and the exterior of the embedding substance was constrained by boundaries and loads, except for the top. The hip implant and embedding substance formed a symmetrical frictional contact with a friction coefficient of 0.3. We used quadratic solid tetrahedral elements to mesh both components. We employed a single element of a linear shell for the strain gauge. The final mesh density was determined through a mesh independence analysis and convergent output parameters with a Poisson ratio (v) of 0.35. This ratio assumes the linear-elastic behaviour of the material. We simulated the original non-cavity design to identify the stress concentration factor. We performed a sensitivity analysis to

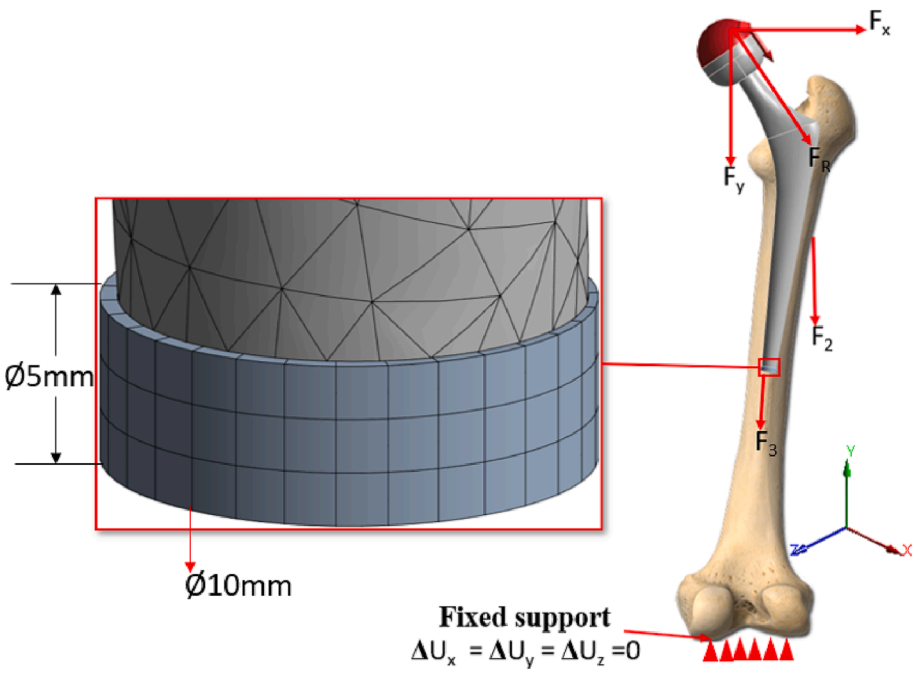

Fig. 1. Illustration of the piezo-acoustic method notion of energy harvesting in the hip implant with 3D printed PLA and fixed support U_x and loading of the FEA design model.

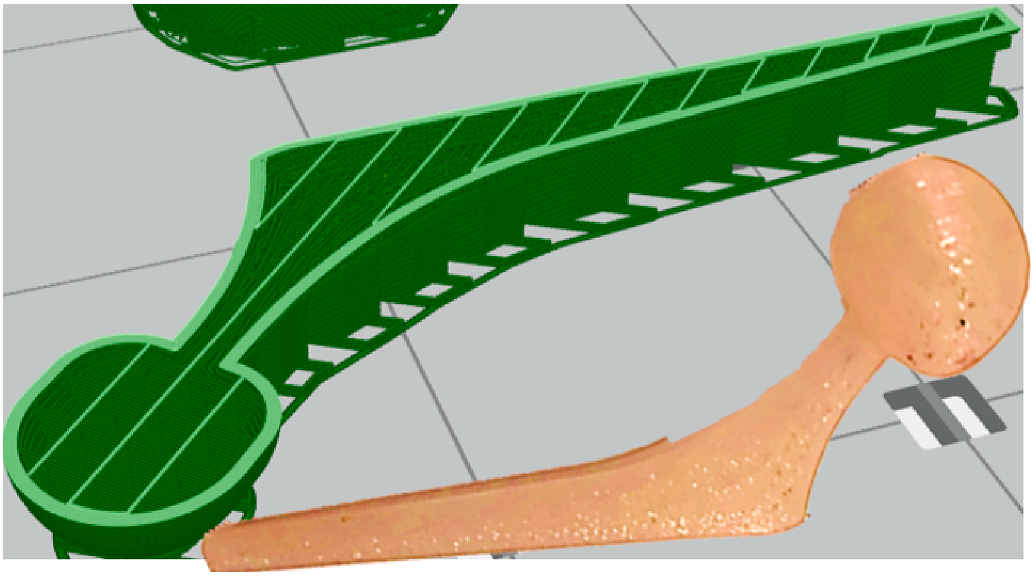

Fig. 2. Slicing of hip implant design for 3D printing and printed hip implant.

understand how input variables affected output stress and strain. We altered Young's moduli by 2.5% after embedding and implanting and considered embedding depths of 1 mm and alignments of 3° during potting. Additionally, we adjusted the axial location of the neck by 0.5 mm to move the head's centre of mass. Our FEA research supports the United Nations Sustainable Development Goal (SDG) 3: Good Health and Well-being by advancing our understanding of orthopaedic implant performance and identifying areas for improvement. Furthermore, using FEA in this study contributes to SDG 9: Industry, Innovation, and Infrastructure by promoting innovative orthopaedic implant development and assessment methodologies.

3.1. Energy harvesting analysis

Implanted devices can potentially obtain power through energy harvesting, which involves converting mechanical or chemical energy into electrical energy from the body's movements. For example, knee, hip, or shoulder movements can generate 49.5mW, 39.5mW, or 2.2mW, respectively [38,39]. However, designing systems that efficiently harvest energy at low gait frequencies (0.5–2 Hz) remains challenging. This section explores how piezoelectric, electromagnetic, and electromechanical sensors can harvest energy. Piezoelectric materials, such as Monolithic PZT, convert mechanical energy into electrical energy through electrical polarisation under mechanical stress. Various

researchers [40,41] have discussed using piezoelectric energy to power intelligent knee implants. In one study, four piezoelectric devices connected to a knee implant produced 11mW of power during in-vitro testing. The same study employed a low-frequency power system with three integrated piezoelectric components to gather energy from tibiofemoral regions for an innovative knee implant. Conversely, a smaller hip implant would require less energy. A hip implant could utilise a piezoelectric ceramic diaphragm to harvest energy from axial loads. In an in-vitro setting, this system generated 0.6mW [42–44]. However, piezoelectric energy harvesters may be unsuitable for hip implants due to their infrequent movement. This research on energy harvesting aligns with the United Nations Sustainable Development Goal (SDG) 3: Good Health and Well-being by investigating innovative ways to power implanted devices, which could improve patients' quality of life. Additionally, this study supports SDG 9: Industry, Innovation, and Infrastructure by promoting cutting-edge technologies and energy-efficient solutions for developing and evaluating orthopaedic implants.

3.2. The equations of piezoelectricity

The piezoelectric effect is a unique phenomenon arising from the linear electromechanical interaction between crystalline materials' mechanical and electrical states. This effect is reversible and stems from electrical and elastic mechanical behaviours. Linear piezoelectricity can be understood through the following two laws that define the material's electrical and mechanical characteristics. Hooke's Law: This law describes the elastic mechanical behaviour of materials. According to Hooke's law, when a flexible material is subjected to stress, it undergoes proportional deformation or strain. The relationship between stress and strain is defined by the material's stiffness, which is a property intrinsic to the material. Linear Electrical Behavior: This law pertains to the electrical response of a piezoelectric material when subjected to mechanical stress. In piezoelectricity, linear electrical behaviour is characterised by the material's ability to generate an electric charge or potential difference in response to mechanical stress or strain. This behaviour is governed by the piezoelectric coefficients specific to the material. Together, these two laws help understand and predict the piezoelectric effect in various materials. By analysing the interplay between the electrical and mechanical properties of crystalline materials, researchers can design and develop innovative applications that harness the unique capabilities of piezoelectric materials:

$$D = \varepsilon E \Rightarrow D_i = \varepsilon_{ij} E_j \tag{1}$$

$$S = sT \Rightarrow S_{ij} = s_{ijkl} T_{kl} \tag{2}$$

The electric charge density displacement electric displacement is denoted by D, the permittivity denotes the free-body dielectric constant, and the electric field strength is denoted by E. The Hooke's law for elastic materials (2), S, strain, s represents compliance under short-circuit conditions, T represents stress, and d represents the direct piezoelectric effect., These relations may be combined into such a matrix. So-called coupled equations can be derived by combining these relations; their **strain-charge form** is as follows:

$$\mathrm{S} = \mathrm{s}\,\mathrm{T} + d^{t}\mathrm{E} \tag{3}$$

$$\boldsymbol{D} = \boldsymbol{d}\,\boldsymbol{T} + \boldsymbol{\varepsilon}\,\boldsymbol{E} \tag{4}$$

We must concentrate on the matrix representation of those equations. A matrix representation of the strain-charge relationship in tetragonal PZT C4V, For example, The strain-charge. Strain-charge for a 4 mm (C4v) crystal class material such as a poled piezoelectric ceramic such as tetragonal PZT or BaTiO3 and a 6 mm crystal class material, for example, can be expressed using the same notation (ANSI IEEE 176):

$$\begin{bmatrix} S_1 \\ S_2 \\ S_3 \\ S_4 \\ S_5 \\ S_6 \end{bmatrix} = \begin{bmatrix} s_{11}^E & s_{12}^E & s_{13}^E & 0 & 0 & 0 \\ s_{21}^E & s_{22}^E & s_{23}^E & 0 & 0 & 0 \\ s_{31}^E & s_{32}^E & s_{33}^E & 0 & 0 & 0 \\ 0 & 0 & 0 & s_{44}^E & 0 & 0 \\ 0 & 0 & 0 & 0 & s_{55}^E & 0 \\ 0 & 0 & 0 & 0 & 0 & s_{66}^E = 2\left(s_{11}^E - s_{12}^E\right) \end{bmatrix} \begin{bmatrix} T_1 \\ T_2 \\ T_3 \\ T_4 \\ T_5 \\ T_6 \end{bmatrix} + \begin{bmatrix} 0 & 0 & d_{31} \\ 0 & 0 & d_{32} \\ 0 & 0 & d_{33} \\ 0 & d_{24} & 0 \\ d_{15} & 0 & 0 \\ 0 & 0 & 0 \end{bmatrix} \begin{bmatrix} E_1 \\ E_2 \\ E_3 \end{bmatrix}$$

$$\begin{bmatrix} D_1 \\ D_2 \\ D_3 \end{bmatrix} = \begin{bmatrix} 0 & 0 & 0 & 0 & d_{15} & 0 \\ 0 & 0 & 0 & d_{24} & 0 & 0 \\ d_{31} & d_{32} & d_{33} & 0 & 0 & 0 \end{bmatrix} \begin{bmatrix} T_1 \\ T_2 \\ T_3 \\ T_4 \\ T_5 \\ T_6 \end{bmatrix} + \begin{bmatrix} \varepsilon_{11} & 0 & 0 \\ 0 & \varepsilon_{22} & 0 \\ 0 & 0 & \varepsilon_{33} \end{bmatrix} \begin{bmatrix} E_1 \\ E_2 \\ E_3 \end{bmatrix}$$

(5)

In finite element analysis, the equations for piezoelectricity can be described using constitutive equations that relate the mechanical stress, strain, electric displacement, and electric field. The constitutive equations for linear piezoelectric materials are as follows:

Strain-stress relationship (Hooke's Law):

$$\sigma\_ij = C\_ijkl * \varepsilon\_kl - e\_ijk * E\_k \tag{6}$$

Electric displacement-electric field relationship:

$$D\_i = d\_ijk * \sigma\_jk + \varepsilon\_ij * E\_j \tag{7}$$

Here, σ_ij represents the stress tensor, ε_kl represents the strain tensor, E_k represents the electric field vector, D_i represents the electric displacement vector, C_ijkl represents the elastic stiffness tensor (relates stress and strain), e_ijk represents the piezoelectric stress coefficients tensor (relates stress and electric field), d_ijk represents the piezoelectric strain coefficients tensor (relates strain and electric field), and ε_ij represents the dielectric permittivity tensor (relates electric displacement and electric field). In finite element analysis (FEA), these constitutive equations are discretised and used to solve for the unknown field variables (displacements, electric potentials) over a meshed domain of numerous small elements. The FEA approach allows for accurately simulating piezoelectric materials' behaviour in complex geometries and under varying loading conditions. By solving these equations for the given boundary conditions and material properties, researchers can gain insights into the performance of piezoelectric devices and optimise their design for various applications.

3.3. Sensitivity and FEA mesh

i. **Types of Finite Elements and Meshing Study:** The finite element analysis utilised tetrahedral elements for most of the model due to their versatility in complex geometries. A total of 100,000 tetrahedral elements were used. For areas requiring higher precision, 10,000 hexahedral elements were applied. After extensive meshing studies, a final mesh size of 0.5 mm guaranteed convergence.
ii. **Sensitivity Analysis:** A comprehensive sensitivity analysis was conducted through several iterations of the finite element model. Various parameters were modified in each iteration, including the material properties, boundary conditions, and loading conditions. In addition, response surface methodologies were used to evaluate the impact of these parameters on the model's output.
iii. **Computational Cost:** The computational cost of the models was carefully monitored. The average CPU time for a single run of the finite element model was approximately 2 h on a standard workstation equipped with an Intel i7 processor and 16 GB of RAM.
iv. **Constitutive Model:** The finite element analysis used an isotropic linear elastic constitutive model. Material properties for the model included Young's modulus of 210 GPa and a Poisson's ratio of 0.3. These values are representative of typical metallic implant materials. The choice of this model reflects the assumption of small deformations and linear material behaviour under the applied loads.

4. Results

To better understand total hip implant loosening before in-vivo studies involving animals or humans, researchers utilise in-vitro laboratory experiments. The in-vitro system does not require a power source or a communication method with the external environment, providing flexibility in assessing implant loosening. Mechanical vibrations and acoustic emissions have been employed to evaluate the loosening of an implant. Multiple research groups[45–47] have applied vibration analysis to detect the loosening of a prosthesis. The methodology involves sending a vibration signal to the femoral condyle and recording the response using an accelerometer, which measures the implant's motion. Only the driving frequency would be observed in a well-fixed prosthesis, where bone and prosthesis move together. The presence of more harmonics in the frequency spectrum indicates implant loosening. A simplified loosening detector utilising vibrations has been developed,

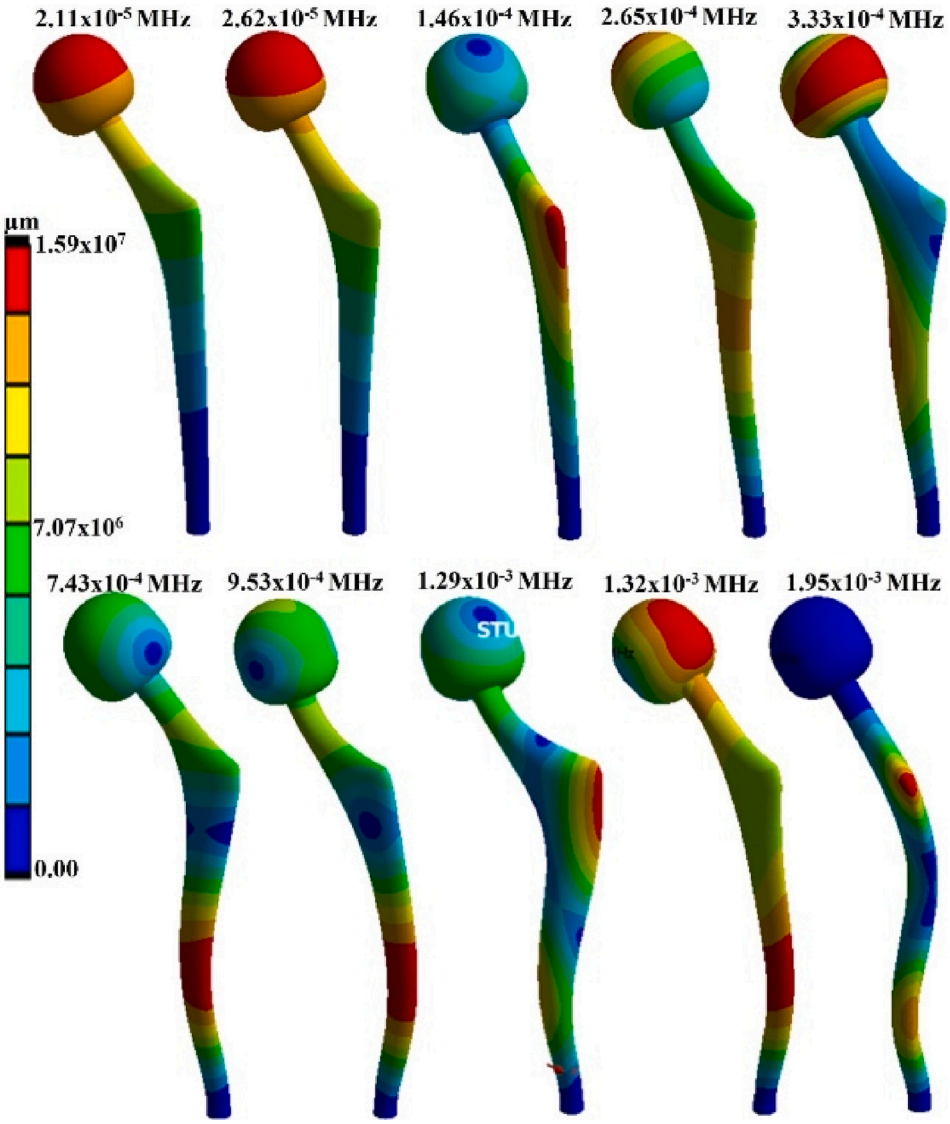

Fig. 3. With a load concentration at the cavity ground, the hip Implant of the deformation in 10 vibration frequency.

relying on an older method for detecting hip implant loosening [48–50]. Two accelerometers were embedded within the prosthesis to monitor the changes in vibration frequency. The applied signal ranged from 500 to 2500 Hz, with loosening states identified between 1500 and 2500 Hz and a frequency shift of 300 Hz. By placing an accelerometer in the implant head, the driving frequency ranged from 500 to 2500 Hz, with a loosening frequency range of 500 to 1500 Hz and a frequency shift of 20 to 100 Hz. An ultrasonic probe was used as a sensor instead of an accelerometer in a similar design. The ultrasonic sensor output exhibited higher harmonic ratios than the accelerometer output, shifting from 200 to 950 mHz [51–53]. Vibration analysis was also used to detect implant loosening but with an accelerometer placed on the skin rather than within the implant. This approach allows assessing multiple patients without needing internal signal conditioning or antennas. The driving frequency range was between 100 and 1500 Hz, while the detection range was from 100 to 450 Hz. Fig. 3 illustrates a load concentration at the base of the cavity, the hip implant deformation at ten different vibration frequencies, with the highest frequency for the 10th sample being 1.9x10^-3. This deformation impacts the piezoelectric material, causing it to generate more energy and voltage, contributing to the UN's goals of sustainable and efficient energy production.

4.1. Testing and FE-model validation

The research results on Testing and FE-model validation, in line with the UN goals, showed that at maximum load, the average strain was 614 m/m, accounting for 3% of the maximum strain. Each load increment increased the strain by 61 m/m. The calculated strain gauge exhibited a 13.1% deviation from the average strain of the three specimens at each load level. The most significant difference was 2300 N (92 m/m). Fig. 4 presents a robust R2 linear regression from experiments and FE simulations (0.997), with a slope of 0.8686 indicating the divergence. Hip implant load concentrations were studied, as stress and strain are closely related to linear-elastic material behaviour. Local load concentrations were identified around the insertion level of the anterior and lateral hip implants. The local singularity generated stress and strain that did not follow the same direction due to contact modification.

Fig. 4 illustrates the comprehensive testing for a representative specimen, detailing the resulting amplitude and power generated. Upper and lower loads were primarily focused on Von Mises stress of maximum value of 55678 MPa. The piezo materials exhibited the highest stress at 0.905 μm/μm and a volt generated of 1.78 volt, slightly inclined to the side with the most significant load gradient. The strain gauge revealed that the strain was more evenly distributed at the maximum von Mises stress when a hollow was created at 163 MPa. The new shape increased the stress level by 2.56 times compared to fatigue data for metallic implant materials, typically reported as stress; piezo base loading was represented as von Mises stress for sensitivity analysis. Fig. 4 does not display the placement and orientation of the strain gauges, as they do not have a significant impact. Any parameters except for and of the region did not influence the tension at the piezo material base; all deviations were 0.2%. A deviation of 0.8% is still considered relatively minor. There were 420 MPa of tension between point C and the front surface of the taper for all modifications that increased stress, amounting to a 1.3% increase (5 MPa). These results contribute to the UN goals of promoting innovation and sustainability and ensuring healthy lives and well-being by offering valuable insights into the performance and validation of hip implant designs.

In line with the UN goals, the research results revealed that the three samples underwent five million testing cycles without noticeable breakage or deformation. The cyclic loading protocol was effectively endured up to the maximum of 18 million cycles. This testing encompassed the repetition and increased the protocol size across eight stages, with one million processes performed at each level. Fig. 5 displays the measured data for a representative sample, demonstrating that the required force level was consistently maintained across various conditions. The displacement curve shows minimal movements, with maximum force values always represented in red and femoral head displacements in blue (Fig. 5). The force-controlled testing environment likely contributed to the minor oscillations observed in the displacement curve. After conducting dynamic testing at the load cell force limit of 5 kN for 18 million cycles without breakage, researchers proceeded with a

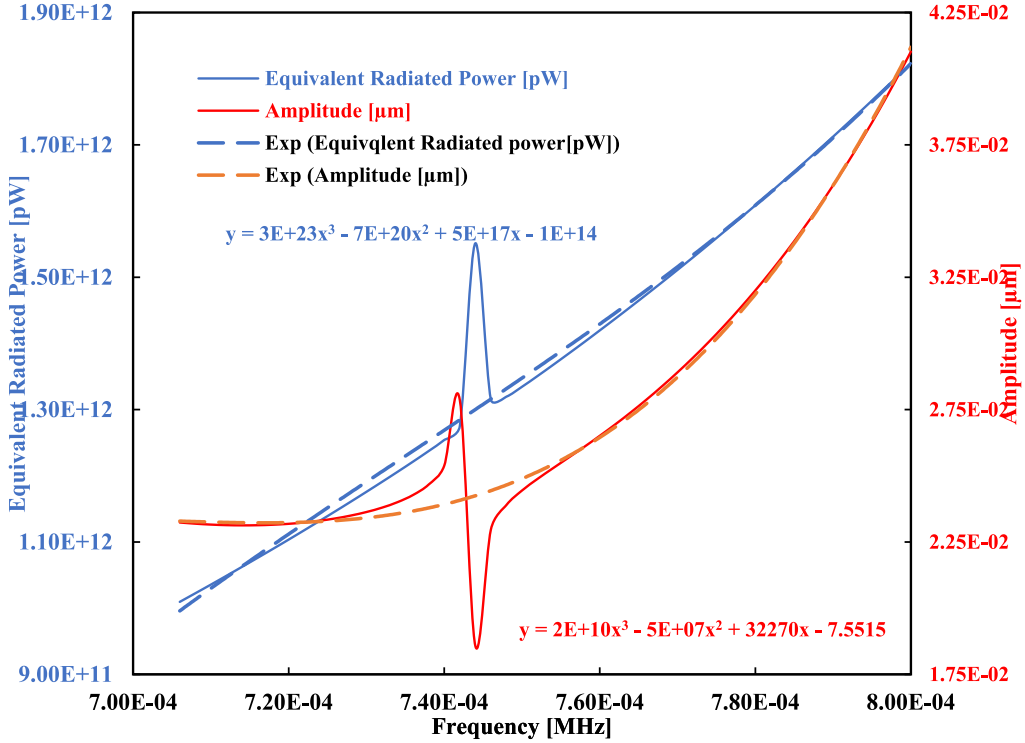

Fig. 4. Complete testing for an exemplary specimen of the resulting amplitude and power generated.

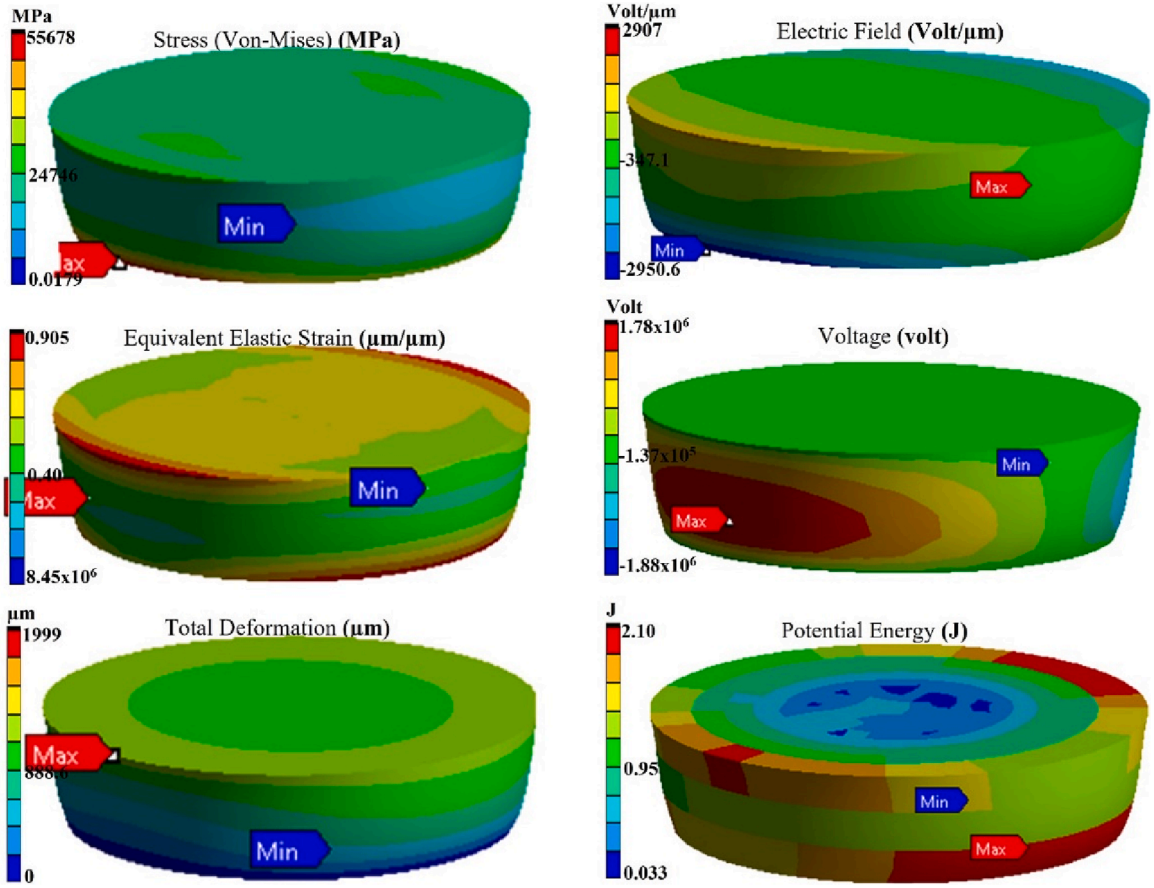

Fig. 5. FE and strain gauge data show a linear relationship; each number result was given one of three strains of the electric field (volt/um) generated, voltage (volt) after compression and potential energy (J).

Table 1
The maximum value of the electric result.

Maximum Values	Values
Equivalent Radiated Power	1823234381834.7
Phase Response Amplitude	436.12
Electric Field Y	2907.34
Potential Energy	2.101
Piezo Impedance Plot Impedance (Amplitude)	7364907.82
Voltage	1177601.88
Total Deformation	1999.27
Equivalent Elastic Strain	0.905
Equivalent Stress	55678.26 (Mpa)

quasi-static experiment using a uniaxial testing machine with an increased test load on the first specimen. The maximum force of 10.1 kN was recorded when the prosthetic head was displaced by 4.74 mm, after which the pressure dropped. The experiment halted at a vertical displacement of 17.43 mm due to the dislodging of the ball ring beneath the actuator.

Fig. 5 reveals significant plastic deformation of the hip implant at the embedding site, but no fracture occurred. Following removal from the embedding media, the maximum vertical displacement was 17.43 mm, and the peak force at 4.74 mm was 10.1kN. Notably, the deformations occurred at the embedding level, with the piezo on the bottom of the strain gauge, which remained connected. Fig. 5 further illustrates the linear relationship between FEA and strain gauge data. Each resulting value was assigned one of three strains of the electric field (volt/um) generated, voltage (volt) after compression, and potential energy (J) (Table 1). These findings contribute to the UN's goals of promoting innovation and sustainability and ensuring healthy lives and well-being by providing valuable insights into the performance and endurance of hip implant designs under various testing conditions.

4.2. Discussion

By the UN goals, the discussion reveals that the material exhibited linear-elastic behaviour, as no stress hot spot exceeded Rp0.2 of 436 MPa. This finding was consistent with the assumptions made for the numerical simulation. Small implant deformations may not have a significant impact on structural stiffness. Fig. 6 demonstrates the relationship between experimental and numerical data, validating the numerical model. However, despite considering sensitivity analysis factors, only two-thirds of the experimental variation of 92 m/m can be accounted for, suggesting that other variables may influence the simulated strain. The location of the strain gauge is critical, as small changes in Young's modulus and head centre point C significantly affect it. The sensitivity analysis may have overlooked additional factors that influence the simulated strain. The bonding process of attaching a strain gauge to the polished hip implant could also introduce inaccuracies due to glue thickness or sticky coatings interfering with strain readings. The hip implant's curvature may have affected bonding. The FE model treated the strain gauge as a single shell and ignored the curvature.

Consequently, the 13.1% discrepancy between calculations and experiments remains unexplained. Simulation-based fatigue data should consider the indicated percentage variation due to the slight standard deviation. The FE analysis results were higher than the actual stresses, implying a conservative estimate. The study improved our understanding of loading by identifying fatigue-prone areas in the implant's simulated stress distribution. Fig. 6 illustrates the harmonic response for phase response with force and displacement. These insights contribute

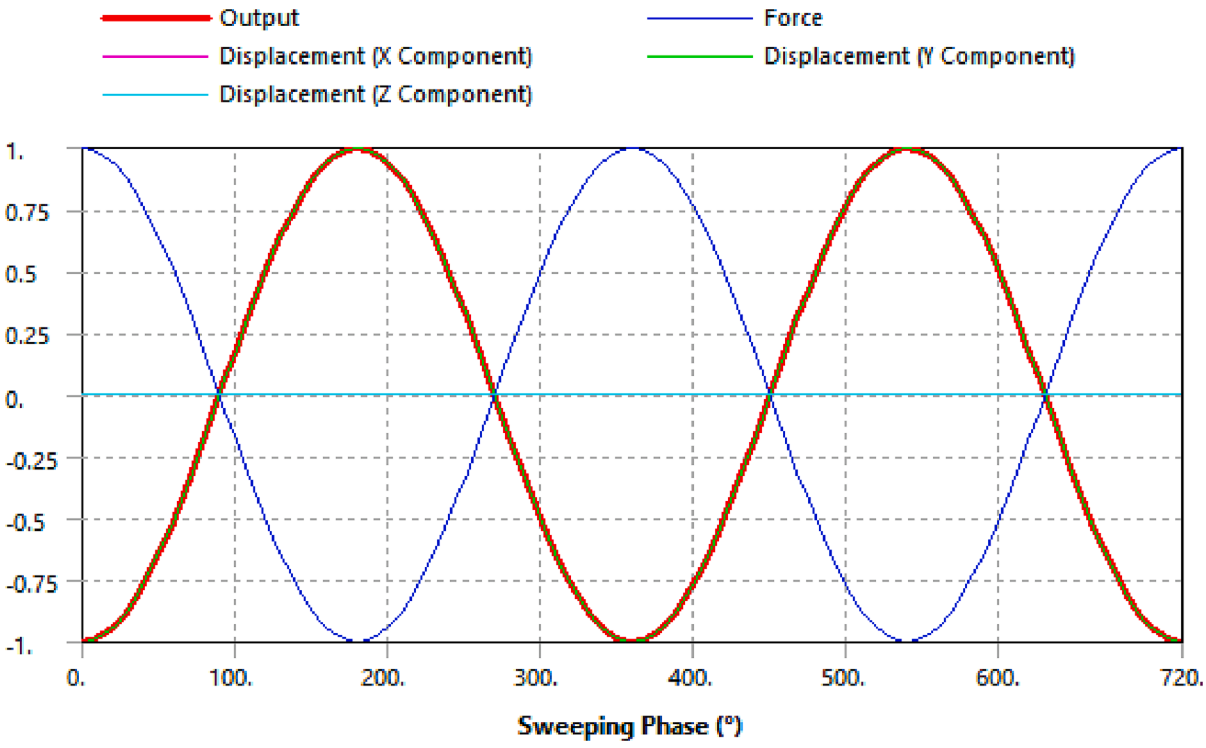

Fig. 6. Harmonic Response for Phase Response with the force and displacement.

to the UN goals of promoting innovation, sustainability, and ensuring healthy lives and well-being by providing valuable information on the behaviour of hip implant materials under various conditions and the factors that may influence their performance.

In line with the UN goals, finite element analysis (FEA) can provide more insights than experimental fatigue testing, which merely determines pass/fail outcomes. By comparing the obtained values with published data, it is possible to refine the design of stress hot zones, such as tensile and compression areas on opposite sides of the upper and lower neck. Research in similar situations supports these findings,

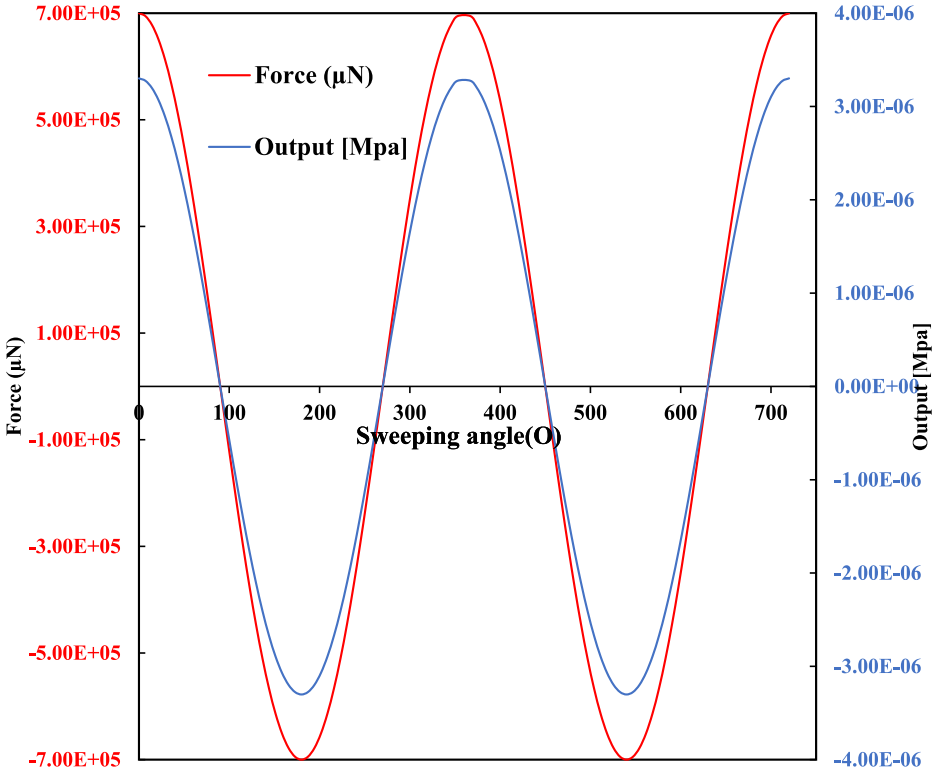

Fig. 7. Test procedure diagram of quasi-static testing for validation fatigue testing was done twice with progressively higher load for generation of sweep angle in respect to force and stress.

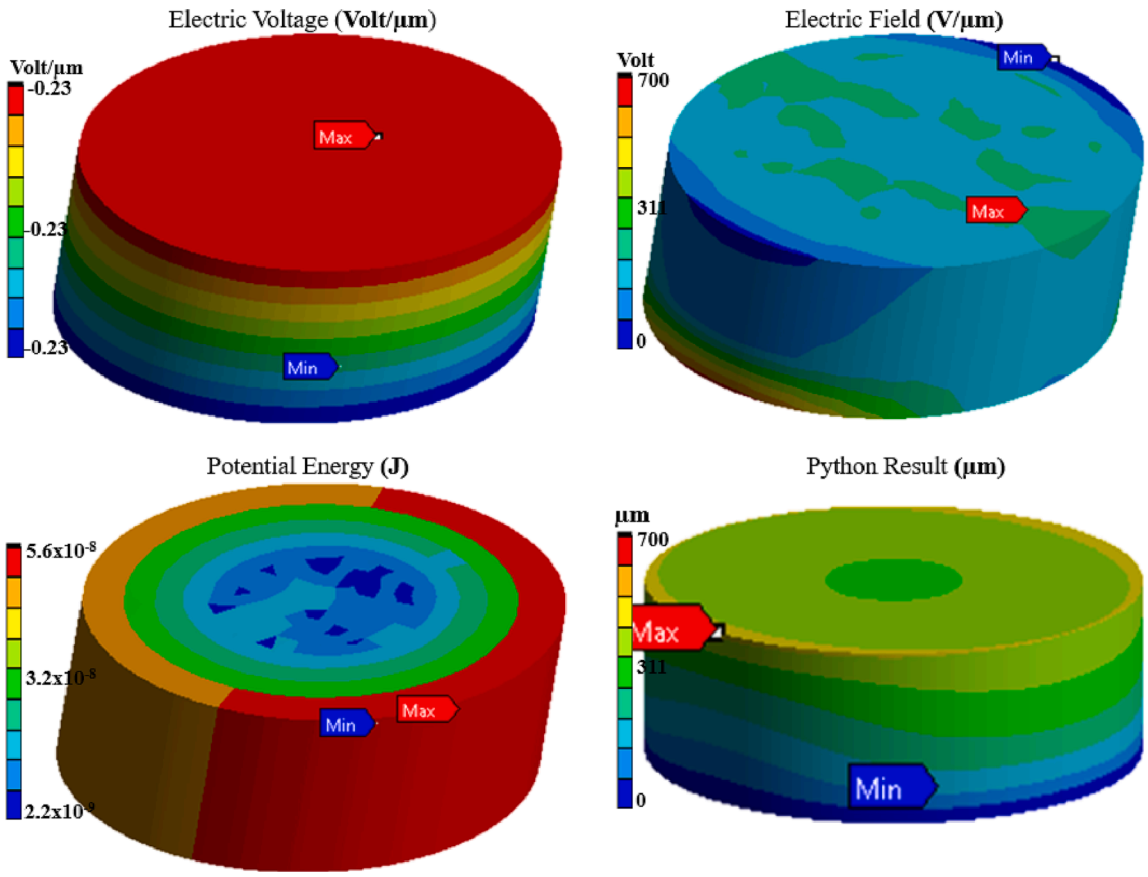

Fig. 8. Different results of electric voltage in electric field generator and energy on the piezoelectric materials.

indicating that a piezoelectric device must be deformed to harvest energy. That piezo-base materials stress concentration was predicted [12,27]. A high gradient suggests the strain gauge may not function correctly, and FEA can offer assistance. The maximum stress was 254 MPa, which the manufacturer understates. The stress maxima are 150 and 60 MPa higher than our previous physiological loading values. The force distribution within the middle of the prosthetic head has changed due to alterations in the embedding method and the absence of housing or piezoelectric elements. According to the sensitivity study, modifying the model did not impact the maximum stress. Strain gauge changes can be disregarded. They only affect numerical values and become more sensitive when the force lever is altered. All values increased by 422 MPa, which is lower than the fatigue data for this material (107 cycles, 10 Hz, in Eagle's medium at 37 °C) but with the same stress ratio of R = 0.1, typical for implant loadings. Since this number depends on manufacturing, surface smoothness, and size [41], it can only provide estimates. Fig. 7 illustrates the test procedure diagram of quasi-static testing for validation. Fatigue testing was conducted twice with progressively higher loads to generate sweep angles concerning force and stress. Fig. 8 displays the various results of electric voltage in the electric field generator and energy in the piezoelectric materials. These findings contribute to the UN goals of fostering innovation, promoting sustainability, and ensuring healthy lives and well-being by providing valuable information on hip implant materials' behaviour under various conditions and the factors that may influence their performance.

In the context of the UN goals, considering the FEA design model variations from quasi-static testing, the 50 MPa difference between the estimated maximum stress at the piezo material base and the reported fatigue result is insignificant. Our experiments were successful, with alignment, embedding, force, and cycles all performing well. The hip implant design allowed for the best possible head offset and increased loading by raising the lever. Although three samples were used instead of the usual six, the research effectively demonstrates how the geometries of energy-harvesting implants impact fatigue failure. The three samples were loaded and run twice, completing the required number of cycles 3.6 times since no implants failed under higher stress. Consequently, implant design modifications are fatigue-resistant, even when the yield threshold of the implant is exceeded during non-static testing. Based on implant morphology, plastic deformation occurred at the embedding level rather than in the piezo material, suggesting higher loading. Although the production process deteriorates the surface, and no fractures develop, rougher surfaces are easier to tread. Fig. 9 illustrates the response of piezoelectric impedance with the displacement and force magnitude. These findings contribute to the UN goals of fostering innovation, promoting sustainability, and ensuring healthy lives and well-being by providing valuable insights into the fatigue resistance and performance of energy-harvesting implants under various conditions. This knowledge can be used to improve implant design, benefiting patients who rely on these devices for improved mobility and quality of life.

5. Conclusion

This study presents a novel approach to energy-harvesting autonomous implants, focusing on improving the performance and sustainability of hip prostheses. We investigated a modified hip implant's structural stress failure strength for piezoelectric energy harvesting. We compared experimental data with estimated stress levels using finite element analysis. This process aids in refining the hip implant design, enhancing load transfer to the piezoelectric element, and increasing energy generation. The development of intelligent orthopaedic implants is being explored as a potential solution to ensure the continuous functionality of implants for an extended period. This research is particularly relevant given the challenges in providing reliable and

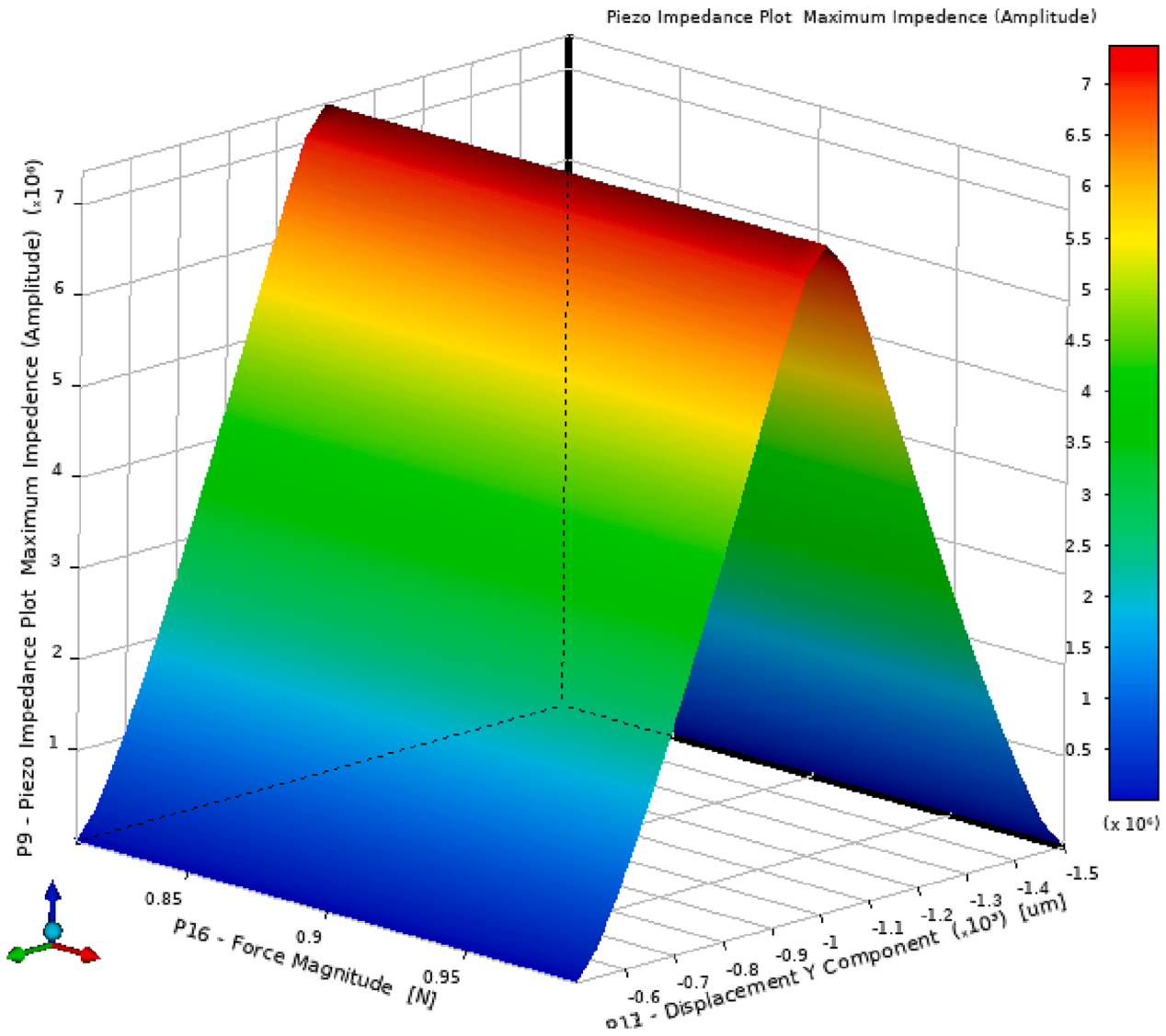

Fig. 9. Response on piezoelectric impedance with the displacement and force magnitude.

easily accessible power to active mechanical components of intelligent prostheses. By applying a unique concept of multi-source energy generation to hip prostheses, we aim to improve the reliability of power supply systems in these devices. Our modified hip implant features three vibration-based harvesters running in parallel to collect energy during an average human stride. This modification demonstrates the feasibility of the concept, capitalising on the angular movements resulting from flexion, extension, and abduction. We measured and analysed the output of each generator across a wide range of frequencies and amplitudes, revealing the potential to harvest up to 55 J/s of helpful power and 1.76 V. With this innovative approach, intelligent hip implants can continue functioning regularly without being disabled and operate without risk. This research contributes to the UN's goals of promoting innovation, ensuring healthy lives and well-being, and fostering sustainability in healthcare solutions. Future studies will further explore energy conversion and fatigue in a complete hip implant design.

Declaration of Competing Interest

The authors declare that they have no known competing financial interests or personal relationships that could have appeared to influence the work reported in this paper.

References

[1] dos Santos MPS, Ferreira JAF, Ramos A, Pascoal R, dos Santos RM, Silva NM, et al. Multi-source Harvesting Systems for Electric Energy Generation on Smart Hip Prostheses. In: Gabriel J, Schier J, Van Huffel S, Conchon E, Correia C, Fred A, et al., editors. Biomed. Eng. Syst. Technol., Berlin, Heidelberg: Springer; 2013, p. 80–96. 10.1007/978-3-642-38256-7_6.

[2] Lange H-E, Bader R, Kluess D. Endurance testing and finite element simulation of a modified hip stem to integrate an energy harvesting system. Proc Inst Mech Eng [H] 2021;235:985–92. https://doi.org/10.1177/09544119211021675.

[3] Oladapo BI, Balogun V. Electrical energy demand modeling of 3D printing technology for sustainable manufacture. Int J Eng 2016;29:954–61.

[4] Qiblawey Y, Chowdhury MEH, Musharavati F, Zalnezhad E, Khandakar A, Islam MT. Instrumented Hip Implant: A Review. IEEE Sens J 2021;21:7179–94. https://doi.org/10.1109/JSEN.2020.3045317.

[5] Lannocca M, Varini E, Cappello A, Cristofolini L, Bialoblocka E. Intra-operative evaluation of cementless hip implant stability: A prototype device based on vibration analysis. Med Eng Phys 2007;29:886–94. https://doi.org/10.1016/j.medengphy.2006.09.011.

[6] Ewald H, Timm U, Ruther C, Mittelmeier W, Bader R, Kluess D, et al. Fifth Int. Conf Sens Technol 2011;2011:494–7. https://doi.org/10.1109/ICSensT.2011.6137029.

[7] Double permanent magnet vibration power generator for smart hip prosthesis - ScienceDirect n.d. https://www.sciencedirect.com/science/article/abs/pii/S0924424711002329 (accessed October 29, 2022).

[8] Oladapo BI, Kayode JF, Karagiannidis P, Naveed N, Mehrabi H, Ogundipe KO. Polymeric composites of cubic-octahedron and gyroid lattice for biomimetic dental implants. Mater Chem Phys 2022;289:126454.

[9] Soares dos Santos MP, Ferreira JAF, Ramos A, Simões JAO, Morais R, Silva NM, et al. Instrumented hip implants: Electric supply systems. J Biomech 2013;46(15):2561–71.
[10] Silva N, Santos P, Ferreira J, Santos M, Reis M, Morais R. Multi-purpose and Multi-source Energy Management System for Biomedical Implants. Procedia Eng 2012;47:722–5.
[11] Morgado ML, Morgado LF, Henriques E, Silva N, Santos P, Santos M, et al. Nonlinear Modeling of Vibrational Energy Harvesters for Smart Prostheses. Procedia Eng 2012;47:1089–92.
[12] Oladapo BI, Zahedi SA. Improving bioactivity and strength of PEEK composite polymer for bone application. Mater Chem Phys 2021;266:124485.
[13] Silva NM, Santos PM, Ferreira JAF, Soares dos Santos MP, Ramos A, Simões JAO, et al. Power management architecture for smart hip prostheses comprising multiple energy harvesting systems. Sens Actuators Phys 2013;202:183–92.
[14] Permanent magnet vibration power generator as an embedded mechanism for smart hip prosthesis - ScienceDirect n.d. https://www.sciencedirect.com/science/article/pii/S187770581000768X (accessed October 29, 2022).
[15] Oladapo BI, Zahedi SA, Ismail SO, Olawade DB. Recent advances in biopolymeric composite materials: Future sustainability of bone-implant. Renew Sustain Energy Rev 2021;150:111505. https://doi.org/10.1016/j.rser.2021.111505.
[16] Oladapo BI, Ismail SO, Adebiyi AV, Omigbodun FT, Olawumi MA, Olawade DB. Nanostructural interface and strength of polymer composite scaffolds applied to intervertebral bone. Colloids Surf Physicochem Eng Asp 2021:627. https://doi.org/10.1016/j.colsurfa.2021.127190.
[17] Oladapo BI, Daniyan IA, Ikumapayi OM, Malachi OB, Malachi IO. Microanalysis of hybrid characterisation of PLA/cHA polymer scaffolds for bone regeneration. Polym Test 2020;83:106341. https://doi.org/10.1016/j.polymertesting.2020.106341.
[18] Morais R, Frias CM, Silva NM, Azevedo JLF, Serôdio CA, Silva PM, et al. An activation circuit for battery-powered biomedical implantable systems. Sens Actuators Phys 2009;156(1):229–36.
[19] Pancharoen K. Hip Implant Energy Harvester. 2017.
[20] Oladapo BI, Oshin EA, Olawumi AM. Nanostructural computation of 4D printing carboxymethylcellulose (CMC) composite. Nano-Struct Nano-Objects 2020;21:100423.
[21] Oladapo BI, Zahedi SA, Ismail SO. Mechanical performances of hip implant design and fabrication with PEEK composite. Polymer 2021;227:123865.
[22] Modelling and Simulation of Automated Hydraulic Press Brake n.d. https://scholar.google.com/citations?view_op=view_citation&hl=en&user=E7toAdYAAAAJ&sortby=pubdate&citation_for_view=E7toAdYAAAAJ:ldfaerwXgEUC (accessed October 30, 2022)..
[23] Morais R, Silva NM, Santos PM, Frias CM, Ferreira JAF, Ramos AM, et al. Double permanent magnet vibration power generator for smart hip prosthesis. Sens Actuators Phys 2011;172(1):259–68.
[24] Oladapo BI, Ismail SO, Bowoto OK, Omigbodun FT, Olawumi MA, Muhammad MA. Lattice design and 3D-printing of PEEK with Ca10(OH)(PO4)3 and in-vitro bio-composite for bone implant. Int J Biol Macromol 2020;165:50–62. https://doi.org/10.1016/j.ijbiomac.2020.09.175.
[25] Oladapo BI, Adeoye AOM, Ismail M. Analytical optimisation of a nanoparticle of microstructural fused deposition of resins for additive manufacturing. Compos Part B Eng 2018;150:248–54. https://doi.org/10.1016/j.compositesb.2018.05.041.
[26] Anguiano-Sanchez J, Martinez-Romero O, Siller HR, Diaz-Elizondo JA, Flores-Villalba E, Rodriguez CA. Influence of PEEK Coating on Hip Implant Stress Shielding: A Finite Element Analysis. Comput Math Methods Med 2016;2016:6183679–10. 10.1155/2016/6183679.
[27] Darwich A, Nazha H, Daoud M. Effect of Coating Materials on the Fatigue Behavior of Hip Implants: A Three-dimensional Finite Element Analysis. J Appl Comput Mech 2020;6:284–95. 10.22055/jacm.2019.30017.1659.
[28] Oladapo BI, Zahedi SA, Omigbodun FT. A systematic review of polymer composite in biomedical engineering. Eur Polym J 2021;154:110534. https://doi.org/10.1016/j.eurpolymj.2021.110534.
[29] Oladapo BI, Zahedi SA, Ismail SO, Omigbodun FT. 3D printing of PEEK and its composite to increase biointerfaces as a biomedical material- A review. Colloids Surf B Biointerfaces 2021;203:111726. https://doi.org/10.1016/j.colsurfb.2021.111726.
[30] Nakahara I, Takao M, Bandoh S, Bertollo N, Walsh WR, Sugano N. In vivo implant fixation of carbon fiber-reinforced PEEK hip prostheses in an ovine model. J Orthop Res 2013;31:485–92. https://doi.org/10.1002/jor.22251.
[31] Oladapo BI, Ismail SO, Zahedi M, Khan A, Usman H. 3D printing and morphological characterisation of polymeric composite scaffolds. Eng Struct 2020;216:110752. https://doi.org/10.1016/j.engstruct.2020.110752.
[32] Oladapo BI, Zahedi SA, Balogun VA, Ismail SO, Samad YA. Overview of additive manufacturing biopolymer composites. 2021.
[33] Oladapo BI, Zahedi SA, Ismail SO. Assessing 3D printing of Poly (ether-ether-ketone) and cellular cHAp to increase biointerfaces as a biomedical material. Colloids Surf B Biointerfaces 2021;111726.
[34] Peek hip implant encourages useful stem cell growth. High Perform Plast 2012:7.
[35] Zhang W, Yuan Z, Meng X, Zhang J, Long T, Yaochao Z, et al. Preclinical evaluation of a mini-arthroplasty implant based on polyetheretherketone and Ti6AI4V for treatment of a focal osteochondral defect in the femoral head of the hip. Biomed Mater Bristol 2020;15(5):055027.
[36] Health Med Week 2021::616.
[37] Oladapo BI, Ismail SO, Ikumapayi OM, Karagiannidis PG. Impact of rGO-coated PEEK and lattice on bone implant. Colloids Surf B Biointerfaces 2022;216:112583.
[38] Oladapo BI, Abolfazl Zahedi S, Vahidnia F, Ikumapayi OM, Farooq MU. Three-dimensional finite element analysis of a porcelain crowned tooth. Beni-Suef Univ J Basic Appl Sci 2018;7(4):461–4.
[39] Yamomo G, Hossain N, Towfighian S, Willing R. Design and analysis of a compliant 3D printed energy harvester housing for knee implants. Med Eng Phys 2021;88:59–68. https://doi.org/10.1016/j.medengphy.2020.12.008.
[40] Uddin MS. On the influence and optimisation of cutting parameters in finishing of metallic femoral heads of hip implants. Int J Adv Manuf Technol 2014;73:1523–32. https://doi.org/10.1007/s00170-014-5946-9.
[41] Xie L, Li X, Cai S, Huang L, Li J. Increased energy harvesting from backpack to serve as self-sustainable power source via a tube-like harvester. Mech Syst Signal Process 2017;96:215–25. https://doi.org/10.1016/j.ymssp.2017.04.013.
[42] Ghomian T, Mehraeen S. Survey of energy scavenging for wearable and implantable devices. Energy 2019;178:33–49. https://doi.org/10.1016/j.energy.2019.04.088.
[43] Smilek J, Hadas Z, Vetiska J, Beeby S. Rolling mass energy harvester for very low frequency of input vibrations. Mech Syst Signal Process 2019;125:215–28. https://doi.org/10.1016/j.ymssp.2018.05.062.
[44] Oladapo BI, Obisesan OB, Oluwole B, Adebiyi VA, Usman H, Khan A. Mechanical characterisation of a polymeric scaffold for bone implant. J Mater Sci 2020;55:9057–69.
[45] Tang Y, Wu C, Wu Z, Hu L, Zhang W, Zhao K. Fabrication and in vitro biological properties of piezoelectric bioceramics for bone regeneration. Sci Rep 2017;7:43360. https://doi.org/10.1038/srep43360.
[46] Oladapo BI, Zahedi SA, Ismail SO, Omigbodun FT, Bowoto OK, Olawumi MA, et al. 3D printing of PEEK–cHAp scaffold for medical bone implant. Bio-Des Manuf 2021;4(1):44–59.
[47] Oladapo BI, Zahedi SA, Adeoye AOM. 3D printing of bone scaffolds with hybrid biomaterials. Compos Part B Eng 2019;158:428–36.
[48] Oladapo BI, Adebiyi AV, Ifeoluwa Elemure E. Microstructural 4D printing investigation of ultra-sonication biocomposite polymer. J King Saud Univ-Eng Sci 2021;33(1):54–60.
[49] Kim J. A Study on the Improvement of the Durability of an Energy Harvesting Device with a Mechanical Stopper and a Performance Evaluation for Its Application in Trains. Micromachines 2020;11:785. https://doi.org/10.3390/mi11090785.
[50] Lange H-E, Arbeiter N, Bader R, Kluess D. Performance of a Piezoelectric Energy Harvesting System for an Energy-Autonomous Instrumented Total Hip Replacement: Experimental and Numerical Evaluation. Materials 2021;14:5151. https://doi.org/10.3390/ma14185151.
[51] Wang J, Zhong C, Hao S, Wang L. Design and Properties Analysis of Novel Modified 1–3 Piezoelectric Composite. Materials 2021;14:1749. https://doi.org/10.3390/ma14071749.
[52] Barbosa F, Ferreira FC, Silva JC. Piezoelectric Electrospun Fibrous Scaffolds for Bone, Articular Cartilage and Osteochondral Tissue Engineering. Int J Mol Sci 2022;23:2907. https://doi.org/10.3390/ijms23062907.
[53] Carter A, Popowski K, Cheng K, Greenbaum A, Ligler FS, Moatti A. Enhancement of Bone Regeneration Through the Converse Piezoelectric Effect, A Novel Approach for Applying Mechanical Stimulation. Bioelectricity 2021;3:255–71. https://doi.org/10.1089/bioe.2021.0019.